

# Degradation mechanism of Alizarin Red in hybrid gas–liquid phase dielectric barrier discharge plasmas: Experimental and theoretical examination

Jing Xue, Li Chen<sup>\*</sup>, Honglin Wang

*The School of Chemical & Energy Engineering, South China University of Technology, Guangzhou 510640, PR China*

Received 14 January 2007; received in revised form 24 May 2007; accepted 29 May 2007

## Abstract

The degradation of the dye Alizarin Red (AR) has been studied in the hybrid gas–liquid dielectric barrier discharge (DBD) plasma. The relationship between the degradation efficiency of AR and the ozone concentration in solutions is analyzed. Based on the bond dissociation energies (BDEs) theory and experimental results, the degradation pathway of AR in DBD plasma is theoretically proposed. It is found that the degradation course consists of three steps in the order of gas-discharge phase, ring-open phase, and mineralization phase. The AR molecule is cleaved into two parts from the weakest bonds  ${}^4\text{C}-{}^5\text{C}$  and  ${}^{12}\text{C}-{}^{13}\text{C}$  after losing  $-\text{NaSO}_3$  first in the gas-discharge phase, when the aqueous ozone concentration is low, leading to low degradation efficiency. Both cleaved transitional groups undergo further oxidation reactions subsequently, forming some unstable intermediates with low molecular weights in the ring-open phase. In this phase the degradation efficiency rises quickly with a sharp increase of the aqueous ozone concentration. Most intermediates are carrying with free radicals, which promote the degradation during the mineralization phase. The main longer-lived species are glyoxylic acid and vinyl formate besides  $\text{CO}_2$ .  
© 2007 Elsevier B.V. All rights reserved.

**Keywords:** DBD plasma; Mechanism; Bond dissociation energies; Alizarin Red; Dye

## 1. Introduction

In the recent years, the degradation of dyes and other organic pollutants has become the focus of environmental remediation efforts. Because of the biorefractory and stable characteristic, more and more dyes are degraded by advanced oxidation technologies, including photocatalysis [1–4], electrochemical degradation [5–7], Fenton oxidation [8], hydrogen peroxide oxidation [9], and plasma oxidation [10,11]. As a new technology, the plasma oxidation method shows several advantages such as: (1) direct in situ production of multiple types of high-reactive chemical species, including molecules and radicals; (2) enhancement and facilitation of degradation reactions through the collisions between high-reactive species and pollutant molecules; (3) without secondary pollution. Compared to other plasma technologies, the dielectric barrier discharge (DBD) plasma has been considered as a promising technology

because of its treatability property of biologically recalcitrant compounds in wastewater, as well as the stability property. Chang et al. [12] have investigated the decomposition of acetone and toluene with glass and  $\text{TiO}_2$  packing pellets combined with a DBD reactor. And they reported that the utilization of  $\text{TiO}_2$  coated pellets cannot improve the decomposition efficiency but can drive the solid byproduct reaction towards mineralization. Kim et al. [13] have reported the decomposition of ethylenediaminetetraacetic acid using DBD plasma with  $\text{He}-\text{Ar}-\text{O}_2$ . And Sato et al. [14] have analyzed the degradation process of methanol.

It's important to analyze the optimal operation parameters, intermediates and the final products during pollutant degradation. However, it is more important to study the mechanism of degradation because it provides fundamental supports for practical applications and theoretic research. The bond dissociation energies (BDEs) theory is a typical approach utilized in theoretically analyzing reaction mechanism. Suegara et al. [15] have revealed the photodegradation pathway of pentachlorophenol with a theoretical proof of BDEs, and confirmed that the predictability is verified through the comparison of the theoretical

<sup>\*</sup> Corresponding author. Tel.: +86 20 87111109; fax: +86 20 87111109.  
E-mail address: celichen@scut.edu.cn (L. Chen).

and experimental results. Dibble [16] has studied the dissociation pathway of 2-hydroxyethoxy radical ( $\text{HOCH}_2\text{CH}_2\text{O}^\bullet$ ) and found two conformers with different BDEs. Wei et al. [17] have investigated the redox reactivities of a number of monolignols by analyzing BDEs, gas-phase ionization potentials, and aqueous oxidation potentials.

However, over the last two decades, most studies about the degradation in DBD plasma focused on the degradability, the technical parameters, and the examination of intermediates or the final products. The degradation mechanism of wastewater in DBD plasma has not been deeply studied. And the relationship between the molecular structure and the degradation pathway in DBD plasma is not clear. In the present study, the degradation of Alizarin Red (AR), a kind of stubborn anthraquinone dye, has been investigated in the hybrid gas–liquid DBD plasma. The degradation mechanism of AR is also proposed on the basis of BDEs theory and the experimental results.

## 2. Materials and methods

### 2.1. Reagents

Analytical grade Alizarin Red was obtained from the Institute of Xinchun Reagent in Tianjin. The chemical structure of AR is shown in Fig. 1. The pH values of AR solution were controlled by  $\text{NaOH-NaH}_2\text{PO}_4$  buffer solution. Analytical grade indicarmin was used as a color indicator for determining the ozone concentration in solution with colorimetry.

### 2.2. DBD plasma reactor

The experimental apparatus consists of a low frequency AC power, a cymometer, an oscillograph, and a DBD reactor, as shown in Fig. 2. The insulating DBD reactor comprises a reacting space and a cooling space. A pair of silver papers in 60 mm diameter is parallel covered on the outer surfaces of reacting space, as a high voltage electrode and a ground electrode, respectively. The reacting space with a diameter of 75 mm and a height of 15 mm is made of insulative glass, above which there is an insulative cooling space. The gap between the high voltage electrode and the water surface was filled with air naturally. A high voltage of 8 kV was applied to generate dielectric barrier discharge plasma. The length of the discharging channels is 8 mm for all experiments. A large number of high-reactive species was generated in the discharging process, which facilitated the degradation of AR.

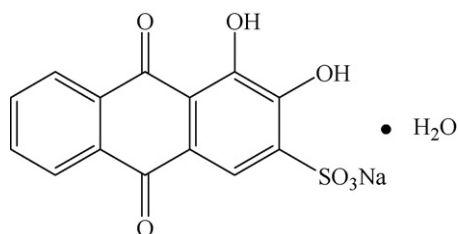
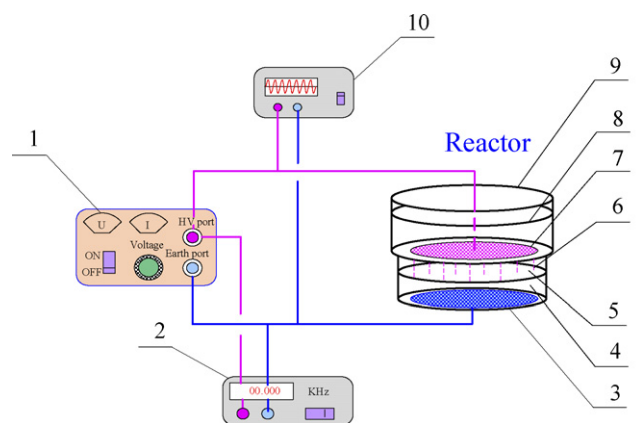


Fig. 1. Chemical structure of Alizarin Red.



1- Low frequency AC power; 2- Cymometer; 3- Ground electrode; 4- Alizarin Red solution; 5- Reacting space; 6- Discharging channels; 7- High voltage electrode; 8- Cooling water; 9- Cooling space; 10- Oscillograph

Fig. 2. Schematic diagram of the experimental apparatus.

### 2.3. Methods and analyses

In each run, 25 ml of 100 mg/L AR solution was treated. The AR solution was added to the reacting space before each run. The gap between the high voltage electrode and the dye solution was filled with air which was excited to generate high-reactive species. The solution conductivity was 5 mS/cm and the input voltage was controlled at 8 kV with the frequency of 15 kHz. The pH values of the samples were measured with a laboratorial pH meter (PHSJ-3F, China). The experiments using the blank solutions were taken under the same conditions as those using the solutions with AR to calculate the concentration of ozone in solutions.

The concentrations of AR solution were calculated by measuring the absorbencies of the solution at 260 nm wavelength using a UV–vis U-3010 Spectrophotometer (HITACHI, Japan). The degradation efficiency  $\eta$  can be calculated as

$$\eta (\%) = \frac{C_0 - C}{C_0} \times 100\% \quad (1)$$

where  $C_0$  and  $C$  are the initial and the final concentration of AR solution, respectively.

The concentration of aqueous ozone can be determined by the decoloration of indicarmin (612 nm, pH below 4) whenever the ozone cannot be measured directly by its UV absorption [18,19]. The values of ozone concentration in solutions were measured by a VIS-723G Spectrophotometer (RUILI, China) at the wavelength of 612 nm when the pH was 2.

The extent of AR mineralization was determined on the basis of total organic carbon (TOC) values measurements, performed by a TOC analyzer TOC-1020A (OI Analytical, USA). The longer-lived species were detected by QP2010 gas chromatography–mass spectroscopy (GC–MS) technique (SHIMADZU, Japan). The analytical conditions are shown in Table 1.

Table 1  
Analytical conditions of GC–MS

GC conditions		MS conditions	
Injection mode	split	Ion source temperature	200 °C
Split rate	20:1	Interface temperature	250 °C
Carrier gas	helium (99.9999%)	Solvent out time	3 min
Sample volume	2 ml	Start time	3.1 min
Injector temperature	270 °C	Start ( <i>m/z</i> )	20
Temperature program		End time	18.33 min
50 °C (2 min)		End ( <i>m/z</i> )	600
220 °C (30 °C/min)		Mode	scan
260 °C (6 °C/min)			
220 °C for 3 min holding			
260 °C for 1 min holding			

### 3. Results and discussion

#### 3.1. Degradation of AR

Before each run, the pH values of AR solution were controlled at 8.4, 7.0, and 5.8, respectively, by the phosphate buffer solution. Fig. 3 shows the variation of the degradation efficiency of AR in the DBD plasma in 40 min. It is obvious that the degradation efficiency increases with discharge time. The degradation efficiency gets the highest value in the solution with pH 8.4, which can reach 99.74% after 40 min. For the solutions with pH 5.8 and 7.0, the degradation efficiencies are 93.78 and 88.55%, respectively, after 40 min. It is also found that there is a tight relationship between the degradation efficiency and the discharging phenomena (Fig. 4). According to Figs. 3 and 4, the degradation process of AR can be divided into three phases: (1) gas-discharge phase; (2) ring-opening phase; (3) mineralization phase.

The first 1 min in the degradation with a weak and sporadic discharge belongs to the gas-discharge phase, when the energy density of the whole plasma area is low. And the UV light and the primary oxide ozone are mainly formed in the gas phase. The concentrations of high-reactive species in the liquid phase are low, which can be explained by the sparse discharging channels

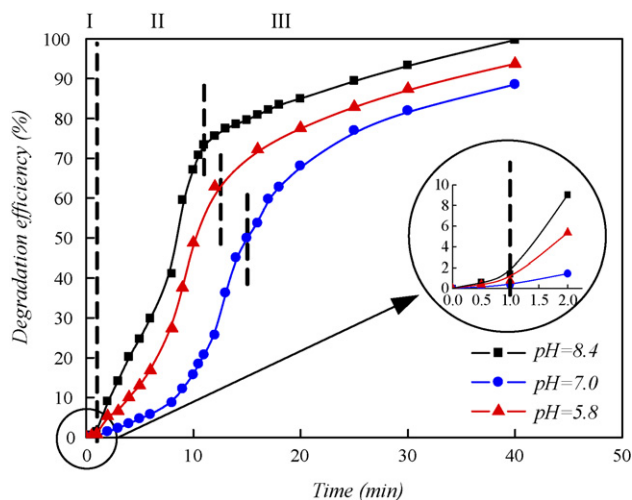


Fig. 3. Variation of the degradation efficiency of AR with discharge time at different pH values in the hybrid gas–liquid phase DBD plasma.

(Fig. 4(I)) and the resistance of mass transfer. Consequently, the degradation efficiencies are low in the first 1 min. And there is no obvious difference in the degradation efficiency of the solutions with different pH values.

Ring-open phase is the crucial step of degradation. In this phase, the aromatic ring is broken down and the degradation efficiency rises quickly. It lasts 11 min in the solution with pH 8.4 compared to 13 and 15 min in the solutions with pH 5.8 and 7.0, respectively. A large number of species are ionized in the discharging area, forming the intense and symmetric discharging channels (Fig. 4(II)). As a result, the concentrations of active species in solutions increase quickly with the mass transfer from the gas phase to the liquid phase, leading to a sharp rise of the degradation efficiency of AR. It indicates that the formation and evolution of discharging channels are important in the plasma reactions.

In the mineralization phase, most of transitional intermediates undergo further oxidation. The discharging channels in this phase become more intense than those in the previous two phases (Fig. 4(III)). That's because some vapor is generated in the discharging space as the result of exothermic reaction. However, the increasing rate of AR degradation in the mineralization phase is lower than that in the ring-open phase because the concentration of residual AR in the solution is low, which decreases the collision probabilities between active species and AR molecules.

#### 3.2. Variation of total organic carbon (TOC)

The TOC values are related to the total concentration of organics in solutions. The variations of TOC reflect the degree of mineralization in the degradation reactions, and the results are presented in Fig. 5.

As shown, the TOC profile shows an immediate decrease in the first 8 min, followed by an increase for about 7 min, and then exhibits a fast decrease. The two inflexions at 8 and 15 min in the TOC curve are named as points V and P. The initial drop behavior can be explained that partial bonds in AR molecule are easily destructed by high-reactive species in a short time. Then some low-molecular-weight intermediates are generated in the solution. They are active because of the free radicals they are carrying with. Thus the intermediates can easily be mineralized to CO<sub>2</sub>, causing the initial decrease of TOC.

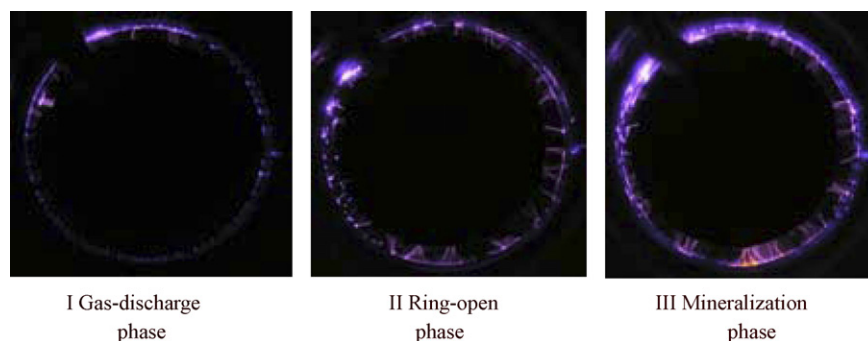


Fig. 4. Discharging phenomena in different phases in the hybrid gas–liquid phase DBD plasma reactions.

However, the TOC values increase to another inflexion P following the point V. The increasing of TOC denotes the formation of some aqueous organics with better solubility [20]. Therefore, it is deduced that some dissolvable intermediates, such as organic acids and alcoholic aldehyde, have been produced in the degradation process. The similar results were obtained by Roig et al. [21] and Kusic et al. [22]. Meanwhile, esters are detected as longer-lived species in our experiments according to the GC–MS results in Section 3.3.2. This confirms the formation of dissolvable organic acid and alcoholic aldehyde. The detailed pathway of the degradation will be discussed in Section 3.4.

The TOC values exhibit a substantial decrease following the inflexion P. It should be attributed to the formation of the large numbers of high-reactive species. All these species facilitate the degradation by colliding with the intermediates. Therefore, more and more covalent bonds are split up to isolated electrons. Then the intermediates with isolated electrons are further mineralized, resulting in the consecutive decrease of the TOC values.

### 3.3. Ozone and longer-lived species

#### 3.3.1. Ozone concentration

In order to study the importance of high-reactive species on AR degradation, the aqueous concentrations of the most primary

oxide, ozone, were analyzed in the experiments using blank buffer solutions without AR. In our experiments, the original  $O_3$  was generated in the gas phase by discharging on  $O_2$  in air.  $O_3$  can dissolve in water easily because of its good solubility. As a kind of essential oxide, ozone promotes the formation of multi-species with high-reactivity, such as  $\bullet OH$ ,  $HO_2\bullet$ ,  $\bullet O_2^-$ , and  $\bullet O_3^-$ . The variations of ozone concentration in the buffer solutions with discharge time at pH 8.4, 7.0, and 5.8 are shown in Fig. 6.

With the same degradation time, the ozone concentration in the solution with pH 7.0 is lower than those in the solutions with pH 8.4 and 5.8. This matches the result shown in Fig. 3, where the degradation efficiency is the lowest in the solution with pH 7.0. Therefore, ozone is an essential oxide in the degradation of AR in DBD plasma reaction.

The ozone concentration in the solution with pH 8.4 is lower than that in the condition of pH 5.8, but Fig. 3 shows the higher degradation efficiency in the solution with pH 8.4. This can be explained by two reasons: (1) the oxidation potential of ozone under acidic conditions is 1.25 V, compared to 2.07 V under alkaline conditions [23,24]. Ozone has stronger oxidative property in the solution with pH 8.4; (2) under acidic conditions, the major reaction is the direct oxidation caused by ozone itself, resulting in the less thorough degradation [25]. On the con-

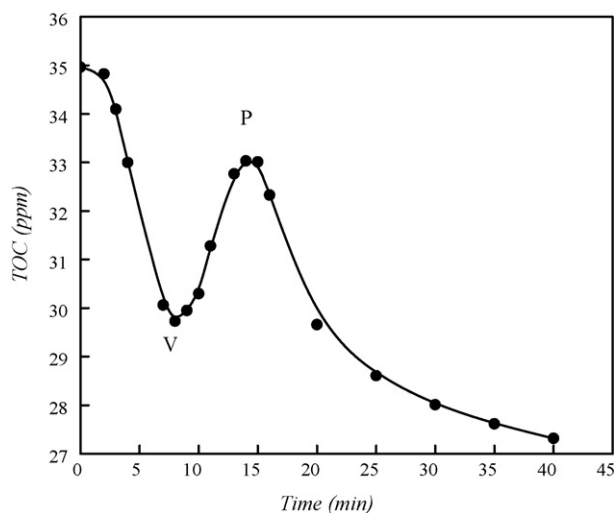


Fig. 5. Variation of TOC values of AR solution with discharge time in the hybrid gas–liquid phase DBD plasma (pH 8.4).

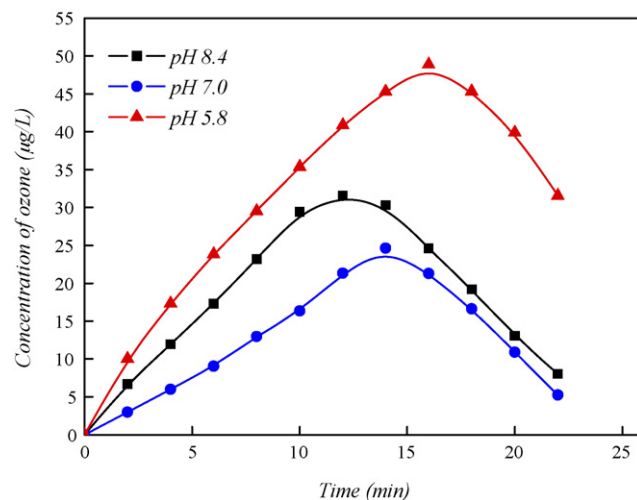


Fig. 6. Variation of ozone concentrations in blank buffer solutions without AR with discharge time in the hybrid gas–liquid phase DBD plasma reactions.

Table 2  
Oxidation potentials of primary high-reactive species [25]

High-reactive species	Oxidation potential (V)
Hydroxyl radical ( $\bullet\text{OH}$ )	2.80
Atomic oxygen (O)	2.42
Ozone in alkaline (O <sub>3</sub> )	2.07
Perhydroxyl radical (HO <sub>2</sub> $\bullet$ )	1.70
Ozone in acid (O <sub>3</sub> )	1.25

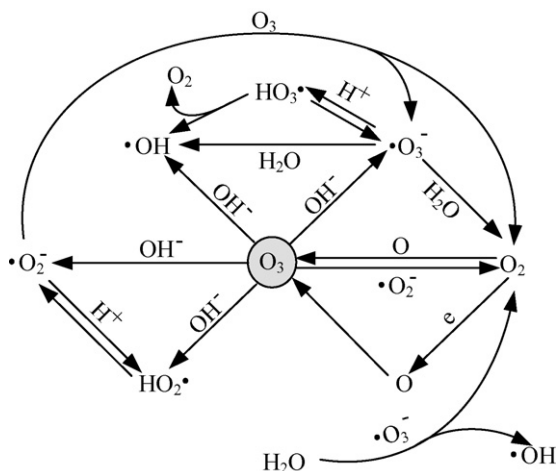
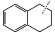


Fig. 7. Schematic diagram of inter-transformations among primary high-reactive species.

trast, under alkaline conditions, it is easier to form  $\bullet\text{OH}$  that has a higher oxidation potential of 2.80 V [23,24]. Under the advantageous circumstances with high oxidation potential the degradation is more complete. Therefore, the higher degradation efficiency has been obtained in the solution with pH 8.4.

In the plasma reaction, the formation and consumption of ozone appear synchronously, leading to a maximum value of ozone concentration in solutions (Fig. 6). The primary reactions with O<sub>3</sub> are listed as formulas (2)–(7) [26–30]. Formulas (2)–(4) describe the generation of O<sub>3</sub> and formulas (5)–(7) exhibit the

Table 3  
Datasheet of chemical bond dissociation energies [31]

Break bonds	BDEs (kcal/mol)	Characteristics of bonds
<b>CH<sub>3</sub>–SH</b>	74.1 ± 4.2	Metastable
<b>CH<sub>3</sub>–S<math>\bullet</math></b>	70.2 ± 1	Metastable
<b>CH<sub>3</sub>–SO<sub>2</sub></b>	21.4	Extremely unstable
<b>CH<sub>3</sub>–CH<sub>2</sub>C<math>\bullet</math>H<sub>2</sub></b>	23.7 ± 1	Extremely unstable
<b>CH<sub>3</sub>–CH<sub>2</sub>O<math>\bullet</math>HOH</b>	24.7 ± 2.5	Extremely unstable
<b>HOCH<sub>2</sub>–CH<sub>2</sub>C<math>\bullet</math>H<sub>2</sub></b>	24.4 ± 2.5	Extremely unstable
<b>CH<sub>3</sub>–CH(OH)C<math>\bullet</math>H<sub>2</sub></b>	20.3 ± 3	Extremely unstable
	72.9	Metastable
<b>CH<sub>3</sub>–CH<sub>2</sub>C<math>\bullet</math>(O)</b>	37.8 ± 3	Extremely unstable
<b>HC(O)–C(O)H</b>	70.7 ± 1.5	Metastable
<b>CH<sub>3</sub>–CH=C<math>\bullet</math>H</b>	25.8 ± 1.6	Extremely unstable

Bold indicates dissociated group.

consumption of O<sub>3</sub>.

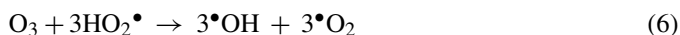
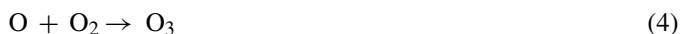


Table 2 lists the oxidation potentials of the primary high-reactive species in solutions [25]. All these species may be formed in the process of the degradation through some reaction pathway [26–30], as shown in Fig. 7. They can act on pollutant directly or form new active groups with other species.

### 3.3.2. Longer-lived species in solutions

The primary longer-lived species in solutions detected by the GC–MS system are glyoxylic acid (HOOCCHO) and vinyl formate (HCOOCH=CH<sub>2</sub>) besides CO<sub>2</sub>, as shown in Fig. 8. The generation of vinyl formate indicates the formation of formic acid and vinyl alcohol in the process of degradation. The results

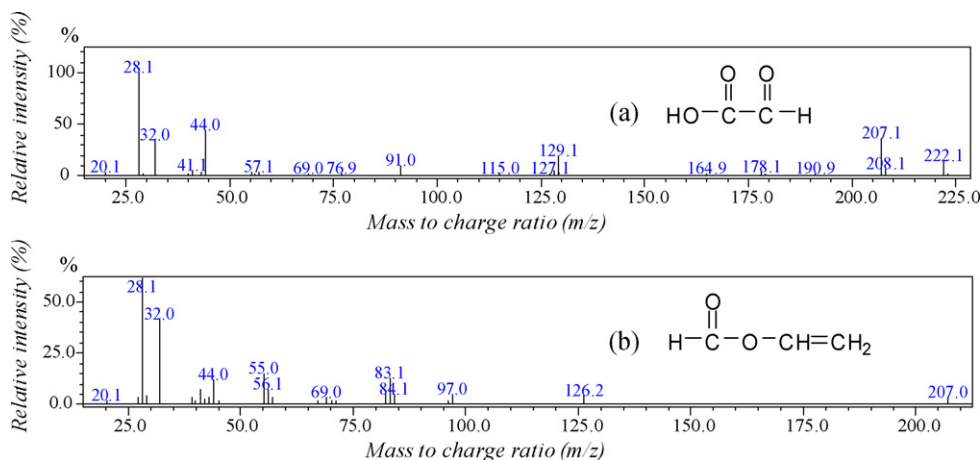


Fig. 8. Mass spectra of major longer-lived species in the hybrid gas–liquid phase DBD plasma reactions ((a) glyoxylic acid; (b) vinyl formate).

show that AR, with a stable molecular structure, can be broken down into several small fragments by the high-reactive species in the DBD plasma degradation.

### 3.4. Degradation mechanism of AR

It is known that most of chemical reactions consist of the breakage of old bonds and the formation of new ones. According to the bond dissociation energies (BDEs) theory, the lower the BDE is, the more active the chemical bond [31]. The primary

fission position of one molecule is the bond with the weakest dissociation energy, where easily losing electrons and being attacked by high-reactive species. Therefore, the intensity of BDEs in AR molecules can determine the plasma degradation pathway. Table 3 lists the dissociation energies of some bonds [31]. Each of them has the similar structure with a certain part of AR molecule. Based on the experimental results above, the BDEs theory, and the ozone and hydroxyl radical chemistry, a degradation mechanism of AR in the hybrid gas–liquid phase DBD plasma has been proposed, as shown in Fig. 9.

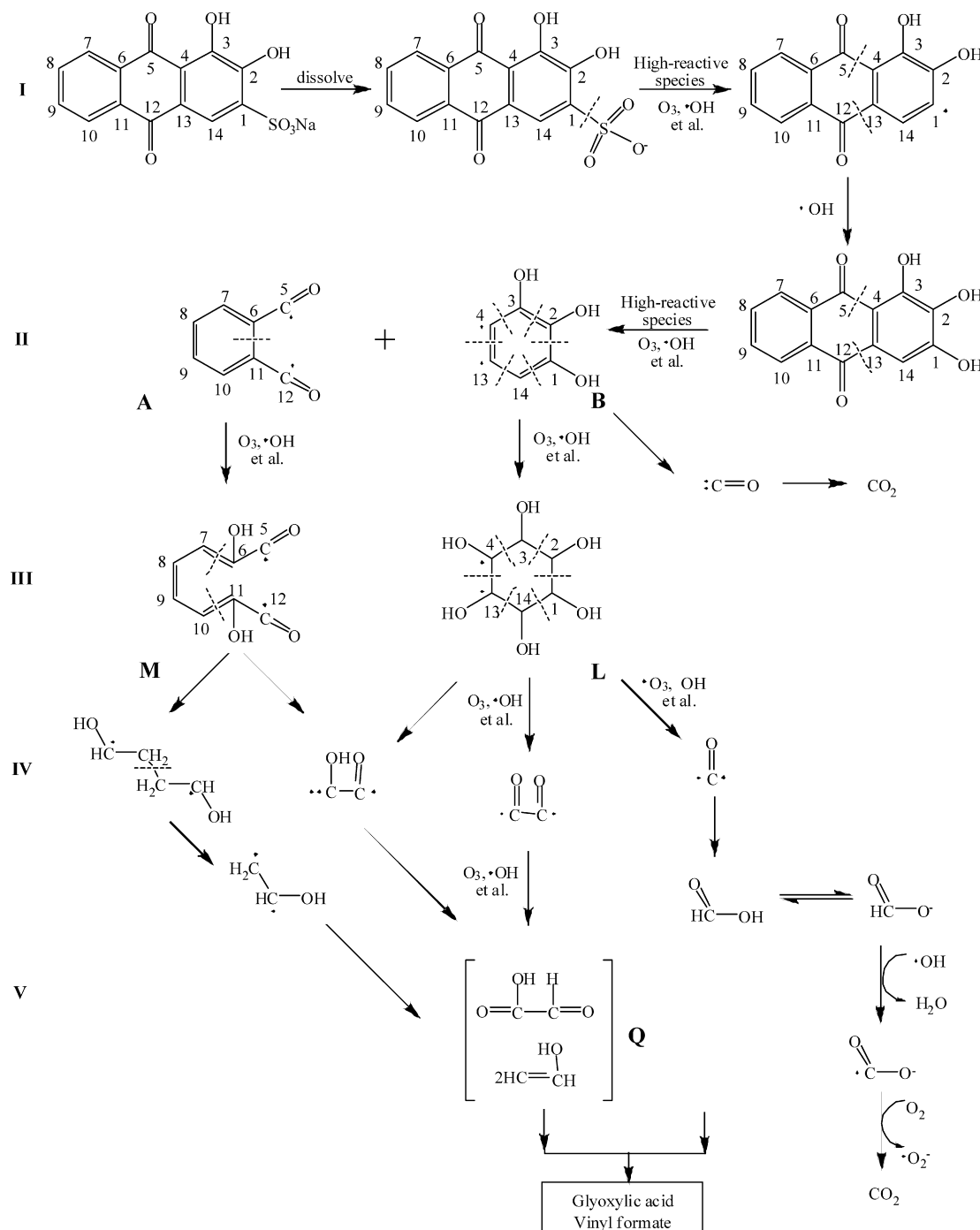
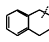


Fig. 9. Degradation mechanism of AR in solutions in the hybrid gas–liquid phase DBD plasma.

The  $\text{SO}_3\text{-Na}$  electrovalent bond is the weakest bond in the AR molecule. It dissociates immediately once the AR dissolves in a solution, leaving an electronegative transitional group as shown in Fig. 9(I). According to Table 3, the dissociation energies of C–S bonds in the groups  $\text{CH}_3\text{-SH}$ ,  $\text{CH}_3\text{-S}^\bullet$ , and  $\text{CH}_3\text{-SO}_2$  are about 74.1, 70.2, and 21.4 kcal/mol respectively. The decrease of C–S BDEs indicates that the intensity of C–S bonds is weakened when the atom S connects with the electronegative atom O. Therefore, the C– $\text{SO}_3^\bullet$  bond in the transitional group is weak enough and can be easily cleaved in the gas-discharge phase (Fig. 9(I)).

For the intermediate group without  $-\text{SO}_3\text{Na}$  generated in the end of gas-discharge phase, the positions  $^4\text{C}-^5\text{C}$  and  $^{12}\text{C}-^{13}\text{C}$  are the easiest bonds to be attacked with two possible reasons. One is the dissociation energy of the bond in the group  is only 72.9 kcal/mol according to Table 3. The low BDE makes the corresponding bonds in AR molecule unstable. The other is that the hydroxyl, as the electron donating group, makes its *ortho*- and *para*-positions,  $^4\text{C}-^5\text{C}$  and  $^{12}\text{C}-^{13}\text{C}$ , easily attacked by the electrophile  $\text{O}_3$  [23]. As a result, the intermediates A and B are formed with the fissions of  $^4\text{C}-^5\text{C}$  and  $^{12}\text{C}-^{13}\text{C}$  (Fig. 9(II)).

According to Table 3, the dissociation energy of  $^\gamma\text{C}-^\beta\text{C}$  bond in the group  $^\gamma\text{CH}_3-^\beta\text{CH}_2^\alpha\text{C}^\bullet(\text{O})$  is only about 37.8 kcal/mol. This is extremely weak because of the *meta*  $^\bullet\text{C}(\text{O})$ . So it is deduced that the  $^\bullet\text{C}(\text{O})$  greatly enhances the activity of the *meta* C–C bond. For the intermediate A, the *meta*  $^6\text{C}-^{11}\text{C}$  bond of  $^\bullet\text{C}(\text{O})$  is the weakest bond, which will be cleaved by  $\text{O}_3$  followed by the connection with hydroxyl radicals shown in Fig. 9(M). In the same way, the intermediate M will be cleaved at the *meta* C–C bonds of  $^\bullet\text{C}(\text{O})$ . The rest may be deduced by analogy until there are some low-molecular-weight intermediates in solutions (Fig. 9(Q)). For the intermediate B, the *ortho*- and *para*-positions of  $-\text{OH}$ ,  $^1\text{C}$ ,  $^4\text{C}$ ,  $^{13}\text{C}$ , and  $^{14}\text{C}$ , will be attracted by  $\text{O}_3$  immediately and then be connected with hydroxyl shown in Fig. 9(L). The intermediate L will be cleaved into several parts through the dashed positions because of the free radicals and hydroxyl radicals it carries with. Lots of low-molecular-weight intermediates with excitons, such as  $^\bullet\text{C}(\text{O})-\text{C}(\text{O})^\bullet$ ,  $^\bullet\text{C}(\text{O})-\text{C}(\text{OH})^\bullet$ , and  $^\bullet\text{C}-\text{C}(\text{OH})^\bullet$ , can be oxidized to  $\text{HCOOH}$  (formic acid),  $\text{HO}(\text{O})\text{C}-\text{C}(\text{O})\text{H}$  (glyoxylic acid), or  $\text{CH}_2\text{CHOH}$  (vinyl alcohol). The formic acid is easily oxidized to  $\text{CO}_2$  by  $^\bullet\text{OH}$  and  $\text{O}_2$ , as shown in Fig. 9(IV) and (V).

It is the ring-open phase when several kinds of intermediates with different molecular weights are produced in solutions shown in Fig. 9(II) and (III). Some low-molecular-weight intermediates, for example,  $\text{C}(\text{O})$ , are easily oxidized into  $\text{CO}_2$  by  $^\bullet\text{O}$  and/or  $\text{O}_3$ . The prompt partial mineralization also indicates the fast increase of degradation efficiency and the initial decrease of TOC. However, the formation of glyoxylic acid, formyl acid, and vinyl alcohol increases the TOC values, which has been mentioned in Section 3.2.

All intermediates experience further oxidation reactions in the process of the mineralization phase. In this phase, several kinds of oxidative reactions take place in solutions, resulting in different kinds of products. Partial organic acid and alcoholic aldehyde undergo a deep mineralization to  $\text{CO}_2$  while partials are combined to form ester, such as vinyl formate. This is con-

sistent with the results that glyoxylic acid and vinyl formate are detected besides  $\text{CO}_2$  (Fig. 9(V)). From the oxidative pathway, a perfect agreement is shown between the analysis of degradation mechanism and the experimental results.

#### 4. Conclusions

In this work, the degradation mechanism of AR in the hybrid gas–liquid phase DBD plasma has been proposed on the basis of BDEs theory and the detection of longer-lived species in solutions. This shows a perfect conformity with the experimental results. The analytical results of ozone concentrations confirm that ozone plays an important role not only in the degradation process of AR but also in the formation of other high-reactive species, such as  $^\bullet\text{OH}$ ,  $\text{HO}_2^\bullet$ ,  $^\bullet\text{O}_2^-$ , and  $^\bullet\text{O}_3^-$ . All these species facilitate the degradation. According to the degradation efficiency and discharging phenomena, the degradation process is divided into three phases: the gas-discharge phase, the ring-open phase, and the mineralization phase. The fission sequence of the bonds in the AR molecule is determined by comparing their BDEs. The AR molecule is cleaved into two parts at  $^4\text{C}-^5\text{C}$  and  $^{12}\text{C}-^{13}\text{C}$  bonds after losing  $-\text{NaSO}_3$  first in the gas-discharge phase, followed by the consecutive fissions of covalent bonds in the ring-open phase. Then most intermediates are further oxidized by the high-reactive species in the mineralization phase. Finally, glyoxylic acid and vinyl formate are detected as the longer-lived species in solutions. The proposal of the mechanism can provide fundamental supports for practical applications and theoretic research on the degradation of wastewater using DBD plasma. And it also reveals that the degradation pathway can be predicted with the BDEs theory.

#### Acknowledgements

We would like to acknowledge financial support from the Guangdong Provincial Science Foundation (No. 2005B50101001) and the Guangdong Provincial Laboratory of Green Chemical Technology.

#### References

- [1] C.C. Liu, Y.H. Hsieh, P.F. Lai, C.H. Li, C.L. Kao, Photodegradation treatment of azo dye wastewater by UV/TiO<sub>2</sub> process, *Dyes Pigments* 68 (2–3) (2006) 191–195.
- [2] N.M. Mahmoodi, M. Arami, N.Y. Limaee, N.S. Tabrizi, Decolorization and aromatic ring degradation kinetics of Direct Red 80 by UV oxidation in the presence of hydrogen peroxide utilizing TiO<sub>2</sub> as a photocatalyst, *Chem. Eng. J.* 112 (2005) 191–196.
- [3] K.V.S. Rao, A. Rachel, M. Subrahmanyam, P. Boule, Immobilization of TiO<sub>2</sub> on pumice stone for the photocatalytic degradation of dyes and dye industry pollutants, *Appl. Catal. B: Environ.* 46 (2003) 77–85.
- [4] H.L. Liu, Y.R. Chiou, Optimal decolorization efficiency of Reactive Red 239 by UV/TiO<sub>2</sub> photocatalytic process coupled with response surface methodology, *Chem. Eng. J.* 112 (2005) 173–179.
- [5] S. Jung, Y. Kim, C. Oh, K. Kang, K. Suh, A combined method of electrocoagulation and electrolysis in the treatment of dye wastewater, *J. Chem. Eng. Jpn.* 8 (12) (2005) 1049–1053.
- [6] D. Rajkumar, B.J. Song, J.G. Kim, Electrochemical degradation of Reactive Blue 19 in chloride medium for the treatment of textile dyeing wastewater

- with identification of intermediate compounds, *Dyes Pigments* 72 (2007) 1–7.
- [7] A. Fernandes, A. Mora, M. Magrinho, A. Lopes, I. Goncalves, Electrochemical degradation of CI Acid Orange 7, *Dyes Pigments* 61 (2004) 287–296.
- [8] A.L. Barros, T.M. Pizzolato, E. Carissimi, I.A.H. Schneider, Decolorizing dye wastewater from the agate industry with Fenton oxidation process, *Miner. Eng.* 19 (1) (2006) 87–90.
- [9] Z.M. Qiu, Y.B. He, X.C. Liu, S.X. Yu, Catalytic oxidation of the dye wastewater with hydrogen peroxide, *Chem. Eng. Process.* 44 (9) (2005) 1013–1017.
- [10] H.J. Wang, J. Li, X. Quan, Decoloration of azo dye by a multi-needle-to-plate high-voltage pulsed corona discharge system in water, *J. Electrostat.* 64 (2006) 416–421.
- [11] A.T. Sugiarto, M. Sato, Pulsed plasma processing of organic compounds in aqueous solution, *Thin Solid Films* 386 (2001) 295–299.
- [12] C.L. Chang, T.S. Lin, Decomposition of toluene and acetone in packed dielectric barrier discharge reactors, *Plasma Chem. Plasma Process.* 25 (3) (2005) 227–243.
- [13] Y.K. Kim, S.A. Kim, S.B. Lee, J.K. Kim, D.W. Kang, Decomposition of ethylene diaminetetraacetic acid using He–Ar–O<sub>2</sub> dielectric barrier discharge, *Plasma Process. Polym.* 2 (3) (2005) 252–255.
- [14] T. Sato, M. Kambe, H. Nishiyama, Analysis of a methanol decomposition process by a nonthermal plasma flow, *JSME Int. J. B: Fluid Trans.* 48 (3) (2005) 432–439.
- [15] J. Suegara, B.D. Lee, M.P. Espino, S. Nakai, M. Hosomi, Photodegradation of pentachlorophenol and its degradation pathways predicted using density functional theory, *Chemosphere* 61 (2005) 341–346.
- [16] T.S. Dibble, Characterization of HOCH<sub>2</sub>CH<sub>2</sub>O and its dissociation pathway, *Chem. Phys. Lett.* 301 (1999) 297–302.
- [17] K. Wei, S.W. Luo, Y. Fu, L. Liu, Q.X. Guo, A theoretical study on bond dissociation energies and oxidation potentials of monolignols, *J. Mol. Struct. (Theochem.)* 712 (2004) 197–205.
- [18] Q.Z. Zhang, P. Wu, B. Liang, R.Y. Wang, Determination of the concentration of ozone in liquid phase, *Ind. Water Treat.* 21 (4) (2001) 30–32.
- [19] H. Bader, J. Hoigné, Determination of ozone in water by the indigo method, *Water Res.* 15 (1981) 449–456.
- [20] D. Wu, J.L. Wang, Partial ozonation of anthracene and characteristic of ozonized products, *Acta Sci. Circum.* 25 (12) (2005) 1586–1589.
- [21] B. Roig, C. Gonzalez, O. Thomas, Monitoring of phenol photodegradation by ultraviolet spectroscopy, *Spectrochim. Acta Part A* 59 (2) (2003) 303–307.
- [22] H. Kusic, N. Koprivanac, A.L. Bozic, Minimization of organic pollutant content in aqueous solution by means of AOPs: UV- and ozone-based technologies, *Chem. Eng. J.* 123 (2006) 127–137.
- [23] J.Y. Chu, C.D. Wu, W.J. Chen, Z.G. Chen, *Ozone Technique and Application*, Chemistry Industry Press, Beijing, 2002.
- [24] B. Sun, M. Sato, J.S. Clements, Optical study of active species produced by a pulsed streamer corona discharge in water, *J. Electrostat.* 39 (1997) 189–202.
- [25] S.A. Tri, I. Shunsuke, O. Takayuki, S. Masayuki, S. Jan, Oxidative decoloration of dyes by pulsed discharge plasma in water, *J. Electrostat.* 58 (2003) 135–145.
- [26] R.E. Buhler, J. Staehelin, J. Hoigne, Ozone decomposition in water studied by pulse radiolysis. 1. HO<sub>2</sub>/O<sub>2</sub><sup>-</sup> and HO<sub>3</sub>/O<sub>3</sub><sup>-</sup> as intermediates, *J. Phys. Chem.* 88 (1984) 2560–2564.
- [27] J. Staehelin, R.E. Buhler, J. Hoigne, Ozone decomposition in water studied by pulse radiolysis. 2. OH and HO<sub>4</sub> as chain intermediates, *J. Phys. Chem.* 88 (1984) 5999–6004.
- [28] P. Vose, W.H. Glaze, D.X. Maddox, Degradation of RDX by various advanced oxidation processes. I. reaction rates, *Water Res.* 32 (1998) 997–1004.
- [29] G. Gottschalk, J.A. Libra, A. Saupe, *Ozonation of Water and Waste Water—A Practical Guide to Understanding Ozone and its Application*, Wiley-VCH Verlag GmbH & Co. KGaA, Berlin, 2002.
- [30] J. Staehelin, J. Hoigne, Decomposition of ozone in water in the presence of organic solutions acting as promoters and inhibitors of radical chain reactions, *Environ. Sci. Technol.* 30 (12) (1985) 1206–1213.
- [31] Y.R. Luo, *Handbook of Bond Dissociation Energies in Organic Compounds*, Science Press, Beijing, 2005.